

Rotordynamics analysis of a double-helical gear transmission system

Siyu Chen · Jinyuan Tang · Yuanping Li · Zehua Hu

Received: 11 September 2014 / Accepted: 27 April 2015 / Published online: 7 May 2015
© Springer Science+Business Media Dordrecht 2015

Abstract The rotordynamics of a double-helical gear transmission system is investigated. The equation of motion of the system with bearing and gyroscopic effect is derived by using the finite element method, in which Timoshenko beam finite element is used to represent the shaft, a rigid mass for the gear. Natural frequencies, mode shapes and Campbell diagrams are illustrated to indicate the effects of gear input speed and time varying mesh stiffness. Besides, effects of mesh stiffness on the critical speed of the gear transmission system are analyzed. The numerical results show that the axial force has significant influence on the natural frequency and the mode shape of the double-helical gear transmission system, for which the mix whirling motion dominates the natural characteristics. There are two higher critical speed curves which increase with the mesh stiffness, but one of them is related to the gyroscopic effect.

Keywords Double-helical gear · Natural frequency · Whirling · Campbell diagram

S. Chen (✉) · J. Tang · Z. Hu
State Key Laboratory of High Performance Complex Manufacturing, Central South University,
Changsha 410083, Hunan, China
e-mail: chsy1324@csu.edu.cn

Y. Li
Key Lab of Disaster Forecast and Control in Engineering,
Ministry of Education of the People's Republic of China
(Jinan University), Guangzhou, China

1 Introduction

Gearing, one of the most important components, is commonly used in automotive, gas turbine and aerospace applications. The double-helical gear, as the main component of a power flow transmission system, has found wide applications in aeroengines and rotorcrafts operating under conditions of high speed and high power, due to its unique characteristics of large contact ratio, smooth transmission and low noise, which enable the system to meet the requirements of heavy duty working conditions. Theoretically, the double-helical gear can accommodate the axial thrust forces and reduce the rigorous request for bearings. In practice, however, the axial vibration excitation resulting from the mesh cannot be neglected and related dynamic analysis is required under high speed and load conditions for two main reasons. The first reason is the existence of manufacturing error. Gearing in most aerospace applications is finished with a grinding process to achieve desired tooth accuracy and surface finish. As the two helices of a double-helical gear cannot be cut simultaneously, spacing error, lead error and apex position error will accompany the grinding process. The second main reason is concerned with the operating conditions (high speed and load) of the double-helical gear set. Generally, the gear set in aerospace application transmits power above the first critical frequency [1, 2]. The deflection of shaft causes gyroscopic effects to vary axial force distribution and potentially exert an

adverse impact on the stability of the gear. Hence, conducting dynamic analysis for a double-helical gear with a thrust bearing to resist axial forces becomes a critical step in the design process, and this is where the rotordynamics come in.

In existing literature, numerous analytical models on spur or helical gears have been developed for the purpose of exploring their dynamic characteristics. First of all, a simple gear dynamic model is adopted to study the dynamic characteristics along the mesh plane. In this case, the effects of shaft and bearing flexibility are simplified or neglected with an underlying assumption. The nonlinear phenomena [3–6] (such as chaos and bifurcation) and parametric resonance [2, 7–9] due to time varying mesh stiffness, gear backlash and friction dominate in the gear dynamic analysis.

Besides, in high speed applications, the coupled lateral and torsional vibrations of a gear transmission system may be different from those obtained in an uncoupled analytical model. The shaft deflection, together with bearing stiffness and damping, may affect the dynamic mesh characteristics of a gear pair. Kang and Kahraman [1] indicate that the shaft flexibility can alter the dynamic response of a gear pair. Furthermore, the coupled lateral and torsional modes are also confirmed experimentally in a planetary gear system [2]. To occupy these phenomena, abundant researches have been done in recent decades. The core concept of the methods adopted is to represent the shaft by a finite element model and introduce the bearing flexibility via a linearized 8-coefficient bearing model. Many results show that the stiffness and damping contained in the shaft and bearing have significant influence on the modal behavior [10]. Lund [11] was the first to consider coupled effects in the torsional–lateral vibrations for a geared rotor system. Subsequently, Iida et al. [12], investigated a simple geared system with coupled torsional and flexural vibrations. Kahraman [13, 14] developed a gear rotor system model, in which the shaft was represented by a finite element model and the flexibility of the bearing was considered. Baud and Velex [15] investigated the dynamics of a gear-shaft-bearing system using a nonlinear gear model. In their study, a nonlinear approach, proposed by Baguet and Velex [16], was applied to analyze the dynamic behaviors of the gear-shaft-bearing model. The shaft was also represented by a finite element model and the

proposed gear element could account for time varying mesh stiffness as well as tooth shape deviations. Later, Baguet and Jacquenot [17] extended the model to helical gears and finite-length hydrodynamic bearing systems. Kang et al. [18] investigated the dynamic behaviors of a gear-rotor system with the effects of viscoelastic support, gear eccentricity, transmission error, and residual shaft bow.

However, literature on double-helical gears is quite rare and the corresponding analysis is limited to geometrical analysis, and load distribution and transmission error under static conditions. Jauregui and Gonzalez (cited in Ref. [19]) studied the axial vibrations in double-helical gears using a single degree-of-freedom dynamic model. Ajmi and Velex [19] presented a model for analyzing the quasi-static and dynamic behaviors of the double-helical gear by taking into account time varying mesh stiffness, gear distortion and shape modifications. In their model, the double-helical gears were constructed by two identical gear elements with opposed helices separated by Euler beam elements. The gyroscopic effect was ignored and the mesh stiffness was not independent since they were all connected to two deformable shafts.

More recently, Sondkar and Kahraman [20] developed a linear dynamic model of a double-helical planetary set to study the effect of staggering of gear teeth. The time varying mesh stiffness and backlash were neglected in their work. Liu et al. [21], used a simple lump-mass model to study the herringbone gear pair with mesh friction and profile error. Among the aforementioned literature, no publication is available on the nonlinear dynamic model of a double-helical gear set with shaft flexibility. There are rare works have been reported on the nonlinear dynamic response of the double-helical gear set especially on the critical speed of this type of gear set under high speed condition. It is generally acknowledged that gear mesh excitations and shaft flexibility coupled with high speeds have resulted in dynamically complicated gear transmission systems. In our established model, the backlash is included. The dynamic behaviors of a double-helical gear set with time varying stiffness and shaft flexibility are studied in the paper. This paper is organized as follows. The system model including gear rotor, shaft, elastic support and gear mesh are proposed in the second section. Subsequently, a consideration of the proposed system model is given in the first part of Sect. 3. Then the effect of

input shaft speed and time varying mesh stiffness on the natural frequencies and critical speeds are investigated in Sect. 3. Finally, a short conclusion is offered in Sect. 4.

2 System model

A simple double-helical gear pair is sketched in Fig. 1. As mentioned above, the shaft flexibility and axial force are considered in the present analysis. The two helices of the double-helical gear pair are modeled separately and connected with a flexible shaft element. The bodies representing the gear and the pinion are assumed to be rigid. The gear mesh flexibility is represented by a linear spring and damper acting on the plane of action normal to the gear tooth surface [20]. In the present work, the dynamic model is developed based on the Finite element method [22, 23]. In the following, the model formulations for the gear, the shaft element and the bearing are described, and then the mass matrices, stiffness matrices and damping matrices (including gyroscopic matrices) of the gear element, the shaft element and the bearing are assembled to obtain the overall system formulation.

2.1 Gear rotor

As mentioned in Ref. [22], it is convenient to consider two angles $\theta_{xi}(i = p, g)$ and θ_{yi} as coordinates describing the angle motion of the rotor as shown in Fig. 2. It is assumed that all the deflections are parallel to the X–Y plane. In this way, θ_{xi} becomes an angular displacement in the yz plane, describing a small

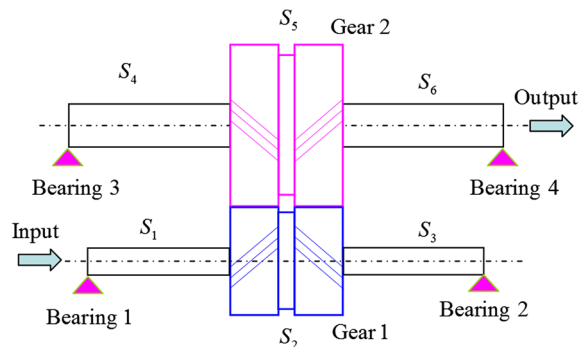


Fig. 1 Sketch of double-helical gear pair

rotation around the x-axis while θ_{yi} becomes an angular displacement in the xz plane describing a rotation around the y-axis. The rotation velocity of gear i (in vector form) can be written as

$$\omega_i = \left[\cos(\Omega_i + \dot{\theta}_{zi}) \dot{\theta}_{yi} + \sin(\Omega_i + \dot{\theta}_{zi}) \dot{\theta}_{xi} \right] \mathbf{X} + \left[\sin(\Omega_i + \dot{\theta}_{zi}) \dot{\theta}_{yi} - \cos(\Omega_i + \dot{\theta}_{zi}) \dot{\theta}_{xi} \right] \mathbf{Y} + \left[(\Omega_i + \dot{\theta}_{zi}) + \frac{\theta_{xi} \dot{\theta}_{yi} - \theta_{yi} \dot{\theta}_{xi}}{2} \right] \mathbf{Z}, \tag{1}$$

where Ω_i is spin speed and $\dot{\theta}_i$ is torsional velocity. Then, the kinetic energy of gear i including the torsional kinetic energy is developed from Shiau and Hwang [24, 25] and written as

$$T_i = \frac{1}{2} m_i (\dot{x}_i^2 + \dot{y}_i^2 + \dot{z}_i^2) + \frac{1}{2} J_{Di} (\dot{\theta}_{yi}^2 + \dot{\theta}_{xi}^2) + \frac{1}{2} J_{Pi} (\Omega_i + \dot{\theta}_{zi}) (\theta_{xi} \dot{\theta}_{yi} - \theta_{yi} \dot{\theta}_{xi}) + \frac{1}{2} J_{Pi} (\Omega_i + \dot{\theta}_{zi})^2. \tag{2}$$

The kinetic energy can be rewritten in matrix form as

$$T_i = \frac{1}{2} \dot{\mathbf{q}}_i^T \mathbf{M}_i^d \dot{\mathbf{q}}_i + \frac{1}{2} \dot{\mathbf{q}}_i^T \mathbf{G}_i^d \dot{\mathbf{q}}_i + \tilde{Q}_i^d(\mathbf{q}_i, \dot{\mathbf{q}}_i) \tag{3}$$

Here,

$$\mathbf{q}_i = [x_i, y_i, z_i, \theta_{xi}, \theta_{yi}, \theta_{zi}]^T \tag{4}$$

Then, with Lagrange equations, we can obtain

$$[\mathbf{M}_i^d] \ddot{\mathbf{q}}_i + \Omega_i [\mathbf{G}_i^d] \dot{\mathbf{q}}_i = \mathbf{F}_i^d \tag{5}$$

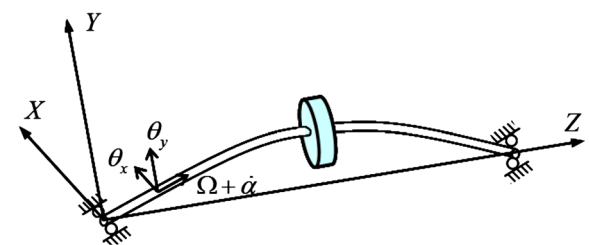


Fig. 2 Typical rotor configuration and coordinate system

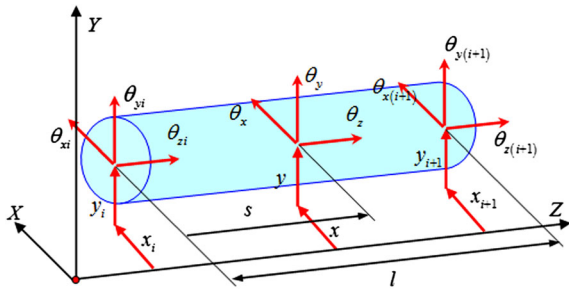


Fig. 3 Shaft beam element and coordinate systems

where

$$\mathbf{M}_i^d = \text{diag}(m_i, m_i, m_i, J_{Di}, J_{Di}, J_{Pi}) \tag{6}$$

$$\mathbf{G}_i^d = \begin{bmatrix} 0 & 0 & 0 & 0 & 0 & 0 \\ 0 & 0 & 0 & 0 & 0 & 0 \\ 0 & 0 & 0 & 0 & 0 & 0 \\ 0 & 0 & 0 & 0 & J_{Pi} & 0 \\ 0 & 0 & 0 & -J_{Pi} & 0 & 0 \\ 0 & 0 & 0 & 0 & 0 & 0 \end{bmatrix} \tag{7}$$

$$\tilde{\mathbf{Q}}_i^d(\mathbf{q}_i, \dot{\mathbf{q}}_i) = \frac{1}{2} J_{Pi} \dot{\theta}_{zi} (\theta_{xi} \dot{\theta}_{yi} - \theta_{yi} \dot{\theta}_{xi}) + \frac{1}{2} J_{Pi} \Omega_i^2 + J_{Pi} \Omega_i \dot{\theta}_{zi} \tag{8}$$

2.2 Shaft element

In this subsection, the Timoshenko beam finite element model theory is applied to construct the shaft as discussed by Nelson [26]. A typical cross section of the element is illustrated in Fig. 3. The deformation of the shaft element can be described by translations $x(s, t)$ and $y(s, t)$ in the X–Y direction and rotations $\theta_x(s, t)$ and $\theta_y(s, t)$ about axes X and Y respectively.

$$\begin{Bmatrix} x(s, t) \\ y(s, t) \end{Bmatrix} = [N_r(s)] \{\mathbf{q}(t)\}, \tag{9}$$

$$\begin{Bmatrix} \theta_x(s, t) \\ \theta_y(s, t) \end{Bmatrix} = [N_b(s)] \{\mathbf{q}(t)\}, \tag{10}$$

$$\theta_z(s, t) = [N_r(s)] \{\mathbf{q}(t)\}, \tag{11}$$

$$z(s, t) = [N_d(s)] \{\mathbf{q}(t)\}. \tag{12}$$

Here, the displacement vector is $\mathbf{q}^T = (x_i, y_i, z_i, \theta_{xi}, \theta_{yi}, \theta_{zi}, x_{i+1}, y_{i+1}, z_{i+1}, \theta_{x(i+1)}, \theta_{y(i+1)}, \theta_{z(i+1)})$ and the spatial constraint matrices are expressed as

$$[N_t(s)] = \begin{bmatrix} N_{t1} & 0 & 0 & 0 & N_{t2} & 0 & N_{t3} & 0 & 0 & 0 & N_{t4} & 0 \\ 0 & N_{t1} & 0 & -N_{t2} & 0 & 0 & 0 & N_{t3} & 0 & -N_{t4} & 0 & 0 \end{bmatrix}, \tag{13}$$

$$[N_b(s)] = \begin{bmatrix} 0 & -N_{b1} & 0 & N_{b2} & 0 & 0 & 0 & -N_{b3} & 0 & N_{b4} & 0 & 0 \\ N_{b1} & 0 & 0 & 0 & N_{b2} & 0 & N_{b3} & 0 & 0 & 0 & N_{b4} & 0 \end{bmatrix}, \tag{14}$$

$$[N_r(s)] = [0 \ 0 \ 0 \ 0 \ 0 \ 0 \ N_{r1} \ 0 \ 0 \ 0 \ 0 \ 0 \ N_{r2}], \tag{15}$$

$$[N_d(s)] = [0 \ 0 \ N_{d1} \ 0 \ 0 \ 0 \ 0 \ 0 \ 0 \ N_{d2} \ 0 \ 0 \ 0], \tag{16}$$

$$N_{r1} = \frac{1}{\phi + 1} (\xi - 1)(2\xi^2 - \xi - \phi - 1),$$

$$N_{r2} = \frac{1}{2} \frac{1}{\phi + 1} l \xi (\xi - 1)(2\xi - \phi - 2), \tag{17}$$

$$N_{t3} = \frac{1}{\phi + 1} \xi (-2\xi^2 + 3\xi + \phi),$$

$$N_{t4} = \frac{1}{2} \frac{1}{\phi + 1} l \xi (2\xi + \phi)(\xi - 1),$$

$$N_{b1} = -N_{b3} = \frac{6}{l(\phi + 1)} \xi (\xi - 1),$$

$$N_{b2} = \frac{1}{\phi + 1} (\xi - 1)(3\xi - \phi - 1), \tag{18}$$

$$N_{b4} = \frac{1}{\phi + 1} \xi (3\xi - 2 + \phi),$$

$$N_{r1} = 1 - \xi, N_{r2} = \xi, \tag{19}$$

$$N_{d1} = 1 - \xi, N_{d2} = \xi \tag{20}$$

$$\xi = \frac{z}{l}, \phi = \frac{12EI}{\mu AGl^2}, G = \frac{E}{2(1 + \nu)}, \tag{21}$$

$$\mu = \frac{6(1 + \nu)(1 + m^2)^2}{(7 + 6\nu)(1 + m^2)^2 + (20 + 12\nu)m^2} \tag{22}$$

where ν is Poisson ratio, and m is the ratio of inner radius to outer radius of the shaft.

As for a 2-node shaft element with 12 degrees of freedom, its kinetic energy including the torsional motion is

$$\begin{aligned}
 T^s = & \frac{1}{2} \int_0^l \rho A (\dot{x}^2 + \dot{y}^2 + \dot{z}^2) ds + \frac{1}{2} \int_0^l \rho I_{ds} (\dot{\theta}_x^2 + \dot{\theta}_y^2) ds \\
 & + \frac{1}{2} \int_0^l \rho I_{ps} (\Omega + \dot{\theta}_z)^2 ds \\
 & + \frac{1}{2} \int_0^l \rho I_{ps} (\Omega_i + \dot{\theta}_z) (\theta_x \dot{\theta}_y - \theta_y \dot{\theta}_x) ds
 \end{aligned}
 \tag{23}$$

The total potential energy of a Timoshenko beam element including bending deflection, shear deformation and torsional deflection is given by

$$\begin{aligned}
 U^s = & \frac{1}{2} \int_0^l \rho EI_{ps} (\theta_x^2 + \theta_y^2) ds + \frac{1}{2} \int_0^l \rho GI_{ps} \theta_z^2 ds \\
 & + \frac{1}{2} \int_0^l \mu GA [(x' - \theta_y)^2 + (y' + \theta_x)^2] ds
 \end{aligned}
 \tag{24}$$

After Lagrange equations are applied, the equation of motion for the un-damped system is derived as

$$[\mathbf{M}^e] \ddot{\mathbf{q}}^e + \Omega [\mathbf{G}^e] \dot{\mathbf{q}}^e + [\mathbf{K}^e] \mathbf{q}^e = 0
 \tag{25}$$

The mass, gyroscopic and stiffness matrices are listed in ‘Appendix 1’.

2.3 Elastic support

In high-speed aerospace applications, gear devices are generally supported with journal bearings. However, a thrust bearing will be recommended to resist axial forces in a double-helical gear transmission system. In addition, the stiffness of a journal bearing is dissimilar to that of a spring support, for the reaction force is not in the same direction as the displacement [27]. There is a component of cross-stiffness in the bearing stiffness matrix as follows,

$$\mathbf{K}_B = \begin{pmatrix} k_{xx} & k_{xy} & k_{xz} & k_{x\theta_x} & k_{x\theta_y} & 0 \\ k_{yx} & k_{yy} & k_{yz} & k_{y\theta_x} & k_{y\theta_y} & 0 \\ k_{zx} & k_{zy} & k_{zz} & k_{z\theta_x} & k_{z\theta_y} & 0 \\ k_{\theta_x x} & k_{\theta_x y} & k_{\theta_x z} & k_{\theta_x \theta_x} & k_{\theta_x \theta_y} & 0 \\ k_{\theta_y x} & k_{\theta_y y} & k_{\theta_y z} & k_{\theta_y \theta_x} & k_{\theta_y \theta_y} & 0 \\ 0 & 0 & 0 & 0 & 0 & 0 \end{pmatrix}
 \tag{26}$$

Here, the subscripts correspond with the coordinate systems of the shaft in Fig. 3. k_{ii} ($i = x, y$) and $k_{\theta_i \theta_i}$ and

k_{zz} are radial and tilting stiffnesses due to the journal bearing respectively. k_{zz} is a simple axial stiffness produced by the thrust bearing. The word “simple” here means that the coupling effects of the thrust and journal bearings are neglected, namely, coupling cross-stiffnesses $k_{zi} = k_{iz} = k_{z\theta_i} = k_{\theta_i z} = 0$. The sixth row and column are zeros because of the free rotation along the shaft axis. In addition, the damping matrix is assumed to be identical with the bearing stiffness matrix.

2.4 Gear mesh process

Figure 4 illustrates the gear mesh model of one side of the double-helical gear. The mesh process is simplified as time varying mesh stiffness and excited by static transmission error. Note that the damping and the static transmission error are not included in Fig. 4. The relative displacement of the gear mesh pair in the direction normal to the tooth surface along the plane of action is represented as [20]

$$\begin{aligned}
 \delta_m = & [(x_p - x_g) \sin \phi + (y_p - y_g) \cos \phi \\
 & + (r_p \theta_{pz} + r_g \theta_{gz})] \cos \beta + [(r_p \theta_{py} + r_g \theta_{gy}) \cos \phi \\
 & + (r_p \theta_{px} + r_g \theta_{gx}) \sin \phi + (z_g - z_p)] \sin \beta - e_{ste}(t).
 \end{aligned}
 \tag{27}$$

Here, ϕ is the transverse pressure angle, β is the helix angle and r_j ($j = p, g$) is the base radius of gear j . Then the mesh force of the gear pair can be written as

$$F_m = k_m (\gamma_{m0} \delta_m + \gamma_{m1} B) + c_m \gamma_{m0} \dot{\delta}_m
 \tag{28}$$

and the index of the backlash function is

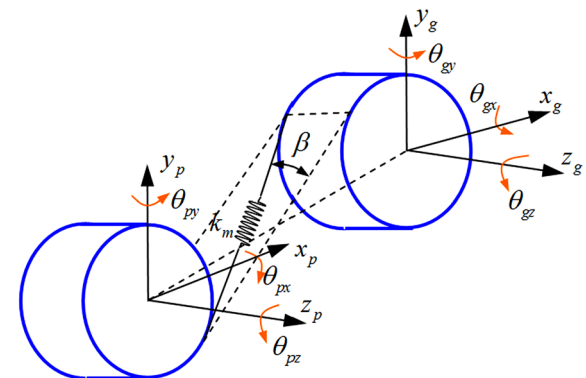


Fig. 4 Sketch of gear mesh model

$$\gamma_{m1} = \begin{cases} -1 & \delta_m > B \\ 0 & \text{else} \\ 1 & \delta_m < -B \end{cases}, \gamma_{m0} = \begin{cases} 1 & |\delta_m| > B \\ 0 & \text{else} \end{cases} \tag{29}$$

In vector form, the mesh force can be rewritten as

$$F_m = k_m \gamma_{m0} \delta_m + c_m \gamma_{m0} \dot{\delta}_m + k_m \gamma_{m1} B \tag{30}$$

$$= k_m \gamma_{m0} \Gamma \mathbf{q} + c_m \gamma_{m0} \Gamma \dot{\mathbf{q}} + k_m \gamma_{m1} B$$

Here,

$$\Gamma = \left(\frac{d\delta_m}{dx_p}, \frac{d\delta_m}{dy_p}, \frac{d\delta_m}{dz_p}, \frac{d\delta_m}{d\theta_{px}}, \frac{d\delta_m}{d\theta_{py}}, \frac{d\delta_m}{d\theta_{pz}}, \frac{d\delta_m}{dx_g}, \frac{d\delta_m}{dy_g}, \frac{d\delta_m}{dz_g}, \frac{d\delta_m}{d\theta_{gx}}, \frac{d\delta_m}{d\theta_{gy}}, \frac{d\delta_m}{d\theta_{gz}} \right) \tag{31}$$

$$\mathbf{q} = (x_p, y_p, z_p, \theta_{px}, \theta_{py}, \theta_{pz}, x_g, y_g, z_g, \theta_{gx}, \theta_{gy}, \theta_{gz})^T \tag{32}$$

$$\mathbf{f}^m = \begin{pmatrix} c_b s & c c_b & -s_b & r_p s s_b & c r_p s_b & c_b r_p \\ c_b s & c c_b & s_b & r_g s s_b & c r_g s_b & c_b r_g \end{pmatrix}^T, \tag{35}$$

$$c_b = \cos \beta, s_b = \sin \beta, c = \cos \phi, s = \sin \phi, \tag{36}$$

The mesh stiffness and damping coefficients are listed in ‘Appendix 2’.

2.5 System equation of gear transmission system

In rotordynamics, the geared rotor system is generally called a branched system [28], as there are two and even more shafts connected by the gear mesh process. Additionally, each shaft rotates at a different speed, and the gyroscopic terms of the shaft element and the disc must account for this. Based on the global coordinate system, the stiffness of a mesh gear pair at nodes i and j can be obtained as

$$i \rightarrow \begin{pmatrix} \vdots & \vdots & \vdots & \vdots & \vdots \\ \cdots & [K_{11}^m]_{6i-5:6i,6i-5:6i} & \cdots & [K_{12}^m]_{6i-5:6i,6j-5:6j} & \cdots \\ \cdots & \vdots & \vdots & \vdots & \cdots \\ j \rightarrow \cdots & [K_{21}^m]_{6j-5:6j,6i-5:6i} & \cdots & [K_{22}^m]_{6j-5:6j,6j-5:6j} & \cdots \\ \vdots & \vdots & \vdots & \vdots & \vdots \end{pmatrix}_{6n \times 6n} \tag{37}$$

Then the equation for the gear transmission system (shown in Fig. 4) is

$$[\mathbf{M}^m] \ddot{\mathbf{q}}(t) + c_m \gamma_{m0} \begin{bmatrix} C_{11}^m & C_{12}^m \\ \text{sym.} & C_{22}^m \end{bmatrix} \dot{\mathbf{q}}(t) + k_m \gamma_{m0} \begin{bmatrix} K_{11}^m & K_{12}^m \\ \text{sym.} & K_{22}^m \end{bmatrix} \mathbf{q}(t) = -k_m \gamma_{m1} \mathbf{f}^m \tag{33}$$

where

$$\mathbf{M}^m = \text{diag} \begin{bmatrix} m_p & m_p & m_p & I_p & I_p & J_p \\ m_g & m_g & m_g & I_g & I_g & J_g \end{bmatrix}, \tag{34}$$

Here, it is assumed that there are n nodes in total. The damping term due to gear mesh can also be constructed in a similar form as Eq. (37). Then every subsystem will be assembled as mentioned above by using the Finite element process to obtain the overall system equation of the double-helical gear transmission system,

$$[\mathbf{M}] \ddot{\mathbf{q}} + ([\mathbf{C}] + \Omega[\mathbf{G}]) \dot{\mathbf{q}} + [\mathbf{K}] \mathbf{f}(\mathbf{q}) = \mathbf{F}(t) \tag{38}$$

where $[\mathbf{M}]$, $[\mathbf{C}]$, $[\mathbf{G}]$ and $[\mathbf{K}]$ are the overall mass matrix, damping matrix, gyroscopic matrix and

stiffness matrix respectively; $\mathbf{f}(\mathbf{q})$ is the nonlinear displacement function due to gear backlash; $\mathbf{F}(t)$ is the gear vibration excitation which includes external torque excitation and internal static transmission error excitation.

3 Numerical analysis

3.1 Consideration of system model

A finite element analysis of the double-helical gear transmission system is given in the following section. Unless otherwise stated, the shaft and the gear are steel and have an elastic modulus of 210 GPa, and a density of 7800 kg/m³ with Poisson’s ratio being 0.3. The geometrical parameters of the gear transmission system corresponding to Fig. 1 are listed in Table 1. The backlash is neglected for the natural frequency analysis.

Generally speaking, the finite element analysis result is basic relative to element size. In order to verify the accuracy of the proposed method above, natural frequencies of a 12-node model and a 42-node model are calculated and listed in Table 2. The results

for the two models agree well with each other, but less computation CPU time is required for the 12-node model. The maximum percentage of the difference between them is 1.38 % at mode 19. Accordingly, in the following analysis, the 12-node model is used to explore the dynamic characteristics of the double-helical gear transmission system.

3.2 Effect of shaft speed

In the first case, the averaged mesh stiffness is adopted, the input pinion shaft speed is set as $\Omega = 5000$ rpm. Table 2 lists the natural frequencies and their corresponding physical descriptions of mode shape for the system with gear mesh effect. It should be noted that the axial freedom is considered in our system model, so the general mode shape diagram is not suitable for the indication of the mode when the axial displacement is dominated. In our work, the three lateral displacements (x , y and z) and bending, rocking and torsion angle displacements (θ_x , θ_y and θ_z) at each node are plotted as the mode shapes.

Figure 5 shows the mode shapes of the first four modes of the geared rotor system. In every subplot, the upper one is for the input shaft distinguished by a superscript 1, and the lower one is for the output shaft distinguished by a superscript 2. In these four mode shapes, the geared rotor presents a conical mode as the curves for lateral displacements (x and y) intersect with the zero amplitude axis. Interestingly, although the isotopic bearing stiffness and damping are used, the geared rotor in the first four mode shapes is dominated by bending and rocking motions. A proper explanation may be that the axial freedom of the shaft element is considered in the proposed system model and that there are opposite axial forces in the two helices of the double-helical gear pair. Moreover, the 1 and 4 modes of the lateral modes of the geared rotor system approximate to the first two modes of the driven gear shaft, and the 2 and 3 modes approximate to the first modes of the driving gear shaft. They are coupled lateral–torsional modes when the gear mesh effect is neglected.

The Campbell diagrams for the cases without geared effect and with geared effect are shown in Fig. 6. The natural frequencies in region (600, 900) Hz are illustrated for convenience. It is observed that in this region, the natural frequencies are less sensitive to

Table 1 System parameters

Components	Values	
	D_{out} (D_{in}) (mm)	Length (mm)
Shaft		
S_1, S_3	95 (75)	115
S_2	150 (120)	80
S_4, S_6	100 (80)	115
S_5	160 (130)	80
Gear	Gear 1	Gear 2
Tooth number	31	24
Normal module	6 mm	
Pressure angle	20°	
Helix angle	35°	
Face width	40 mm	
Mean mesh stiffness	1.855×10^8 N/m	
Bearing	Bearing 1–2	Bearing 3–4
k_{xx}, k_{yy} (N/m)	2×10^8	2×10^8
k_{zz} (N/m)	1×10^8	1×10^8
k_{θ_x, θ_y} (Nm/rad)	1×10^6	1×10^6

Table 2 Natural frequency and mode description for the geared rotor system ($\Omega = 5000$ rpm)

	12 Nodes		42 Nodes	Error
	Natural frequency/kHz	Damping ratio	Natural frequency/kHz	Natural frequency error (%)
0	0	–	–	–
1	0.6241	0.0171	0.6245	0.06
2	0.6529	1.0000	0.6515	0.21
3	0.6634	1.0000	0.6640	0.09
4	0.6991	1.0000	0.7011	0.28
5	0.7435	1.0000	0.7392	0.57
6	0.7581	0.0340	0.7573	0.11
7	0.7713	0.0337	0.7761	0.62
8	0.7969	0.0322	0.7963	0.08
9	0.7970	0.0319	0.7965	0.06
10	0.8358	0.0359	0.8351	0.08
11	0.8561	1.0000	0.8563	0.02
12	0.8599	1.0000	0.8600	0.01
13	0.9901	1.0000	0.9901	0.00
14	0.9915	1.0000	0.9906	0.09
15	1.9654	0.0017	1.9563	0.46
16	2.0631	0.1088	2.0549	0.39
17	2.1422	0.1105	2.1386	0.17
18	2.1511	0.0926	2.1551	0.19
19	2.4745	0.0761	2.4404	1.38

the rotation speed. Moreover, the mode damping ratios for modes 2–5 are critical which are equal to 1. Therefore, the system vibration amplitude will be attenuated seriously where the resonance is close to these natural frequencies, which has no damage to the gear system. In the Campbell diagrams, the pair of natural frequencies corresponding to the critical damping ratio will inversely bifurcate to a single natural frequency as shown in Fig. 6.

Now, a high frequency region (1900, 2500) Hz is considered, and the Campbell diagram is shown in Fig. 7. Five natural frequencies or modes are detected in this region, and they are followed by mode 15 to mode 19 listed in Table 2. Obviously, a frequency veering phenomenon [10, 29] is observed between curves corresponding to mode 17 and 18 around 6000 rpm. After the veering phenomenon occurs, the frequency curves, instead of crossing, swap their trends and maintain continuity as the speed increases. Although the frequency veering appears in the present model, the whirl direction of the two shafts is still the same. This is different from a general rotor case as

noted in Ref. [29] since only the mode shape has changed at the veering point.

The thin dashed line denoted by SWL represents the synchronous whirl line, which is corresponding to mesh frequency in the gear dynamics analysis. The intersection point between the SWL and the natural frequency curve is defined as a critical speed in rotor dynamics. Five critical speeds are detected in Fig. 7 and their corresponding mode shapes are shown in Fig. 8 where the thick lines show the shaft centerline shape at the maximum displacement. As the shafts vibrate, they move from this position to the same location on the opposite side of the un-displaced centerline, and then move back [30]. In Fig. 8, the left is 3D mode shape and the right is a projection on the x – y plane. It can be found that they are all coupled lateral–torsional modes. When the input pinion shaft speed approximates 3804 rpm (1965.4 Hz), the input pinion-shaft refers to cylindrical mode and conical mode (defined in Ref. [30]) for the output gear-shaft. The ratio of the length of the minor axis to the length of the major axis of the ellipse is very small. However,

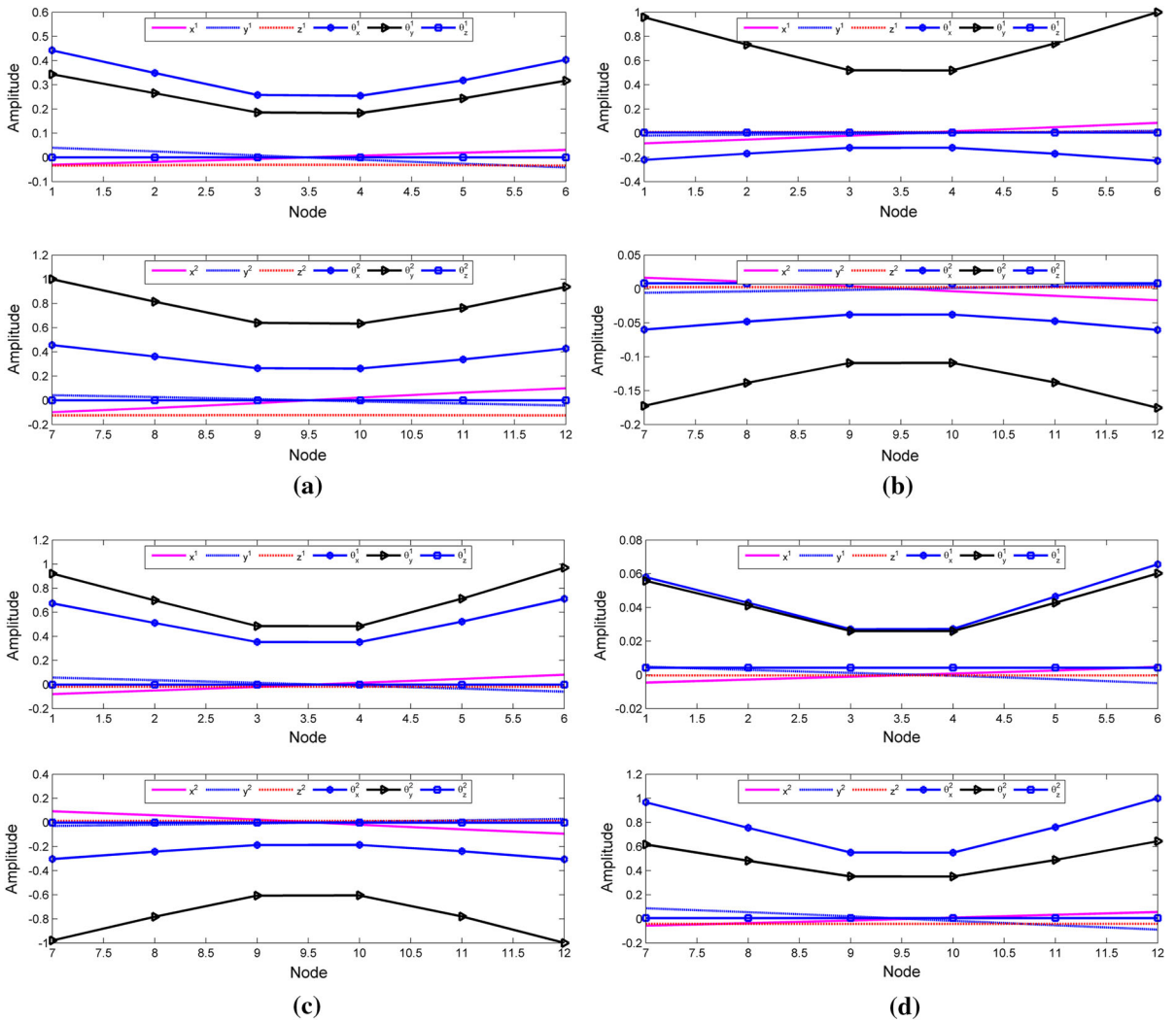


Fig. 5 Mode shapes of the first four lateral modes. **a** 624.9 Hz, **b** 652.9 Hz, **c** 663.4 Hz, **d** 699.1 Hz

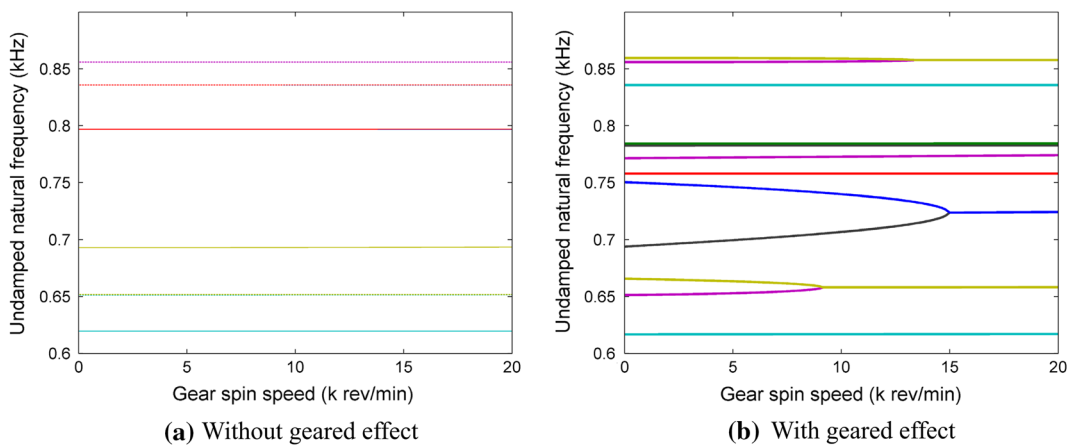


Fig. 6 Campbell diagram in region (600, 900) Hz

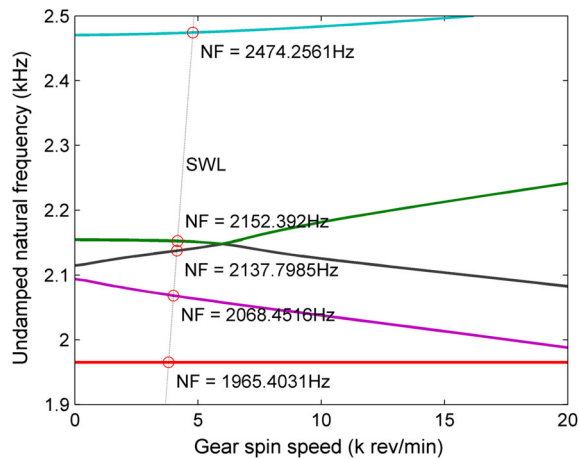


Fig. 7 Campbell diagram in region (1900, 2500) Hz

the two shafts are both a combination of forward and backward motions. The bending motion between the two helices of the output gear is obvious.

3.3 Effect of time varying mesh stiffness

In the preceding section, the time averaged mesh stiffness is used. However, the mesh stiffness will be varied due to the variation of contact position in the mesh process. The mesh stiffness, which is modeled as an internal parametric excitation in numerous studies [3–6], is generally neglected in the geared rotor dynamics analysis, especially in the gear whirling analysis. In the present section, the effects of mesh stiffness on the critical speed of the geared rotor system are illustrated in Fig. 9. For comparison, only the critical speeds appearing in region (1700, 2600) Hz are considered. In Fig. 9, the five curves from bottom to top are indicated by Ncs1 to Ncs5 successively. It can be seen that the critical speed curve Ncs5 increases linearly with the mesh stiffness. However, the critical speed curve Ncs1 no longer monotonically increases with the mesh stiffness, the reason for which is that the action of the special frequency veering occurs when the mesh stiffness is changed. Moreover, a comparison between Figs. 9 and 7 can yield the following findings: (1) The critical speed curve Ncs1 is less sensitive to the gear shaft spin speed and gyroscopic effect, which can be contributed to the torsional motion of the gear pair; (2) The effect of mesh stiffness on Ncs2, Ncs3 and Ncs4 can be neglected, but the gyroscopic effect is implied in these critical speeds; (3) Ncs5 is a coupled

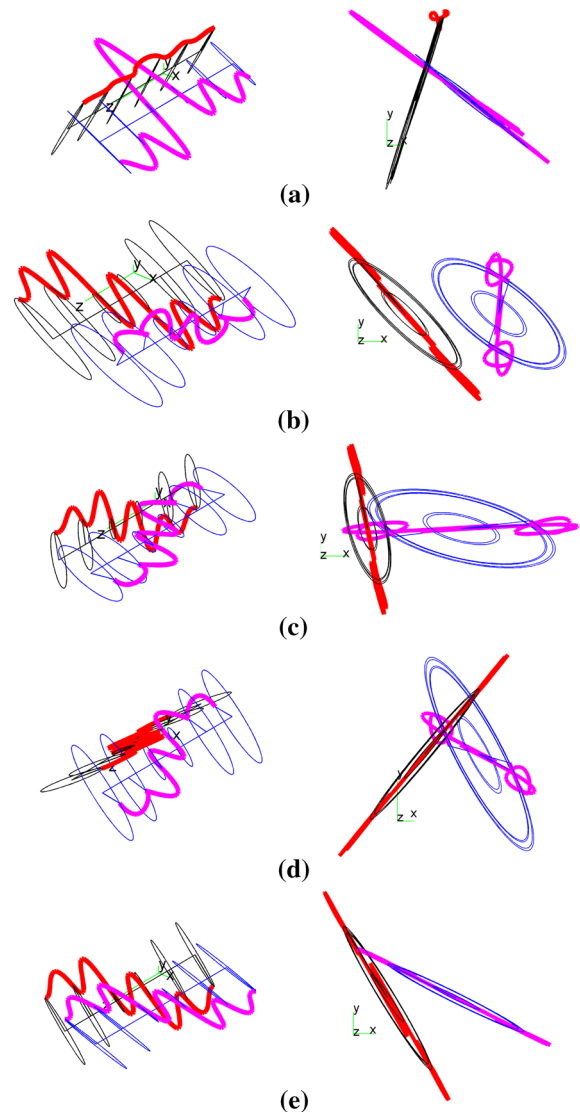


Fig. 8 Mode shape for critical speed. **a** 1965.4 Hz; **b** 2068.5 Hz; **c** 2137.8 Hz; **d** 2152.4 Hz; **e** 2474.3 Hz

result of the gear mesh stiffness and the gyroscopic effect of the system.

4 Conclusions

The rotordynamics of a double-helical gear transmission system was investigated. A model for the shaft element with 2 nodes and 12 degrees of freedom was built to meet the need of double-helical gear analysis, since the axial force is an important factor and cannot

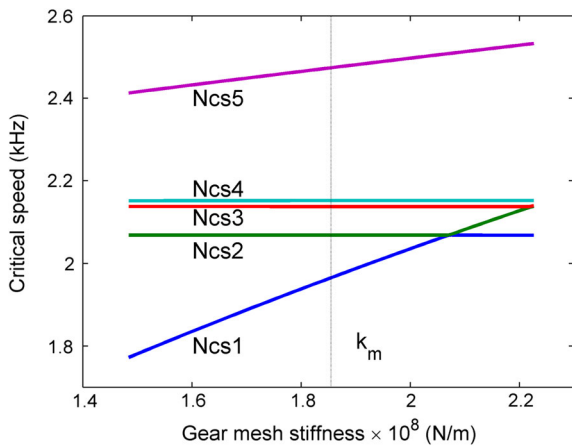


Fig. 9 Effect of gear mesh stiffness on critical speed

be neglected. The equation of motion of the system was derived by using the finite element method, in which Timoshenko beam finite element was used to represent the shaft, a rigid mass for the gear. The gyroscopic effects of the shaft and the gear were also included in the present model. A simple bearing stiffness and a damping matrix were used to explore the effect of the journal bearing as an elastic support boundary. Natural frequencies, mode shapes and Campbell diagrams were illustrated to indicate the effects of gear input speed and time varying mesh stiffness. Meanwhile, effects of mesh stiffness on the critical speed of the gear transmission system were also analyzed. The main findings of the present paper are concluded as follows:

1. The axial force has significant influence on the natural frequency and the mode shape of the double-helical gear transmission system. The mix whirling motion dominates the natural characteristics of the transmission system.
2. Although the isotopic bearing stiffness and damping are used, and the gear pair is assembled

symmetrically, the geared rotors are dominated by bending and rocking motions, which may be attributed to the action of the axial force in the shaft element. The coupled lateral–torsional modes occur in this system.

3. Same as general rotordynamics, frequency veering is detected in the double-helical gear transmission system. One special frequency veering occurs at a higher rotational speed when the gear mesh stiffness is varied.
4. The sensitivity of higher critical speeds to the mesh stiffness is distinguished. Two higher critical speeds increase with the mesh stiffness, but one of them is related to the gyroscopic effect. This is of importance when the operating speed (tooth mesh frequency) of the gear system falls in this range.

Acknowledgments The authors gratefully acknowledge the support of the National Science Foundation of China (NSFC) through Grants Nos. 51305462 and 51275530.

Appendix 1

Mass and stiffness matrices for the shaft beam element are listed as follows:

Mass matrix \mathbf{M}^e

The mass matrix consists of three parts, which can be represented as

$$\mathbf{M}^e = \mathbf{M}_T^e + \mathbf{M}_R^e + \mathbf{M}_\theta^e \tag{39}$$

1. Translational mass matrix \mathbf{M}_T^e

$$\mathbf{M}_T^e = \mathbf{M}_{T1}^e + \phi \mathbf{M}_{T2}^e + \phi^2 \mathbf{M}_{T3}^e \tag{40}$$

Here,

$$\mathbf{M}_{T1}^e = m^T \begin{pmatrix} 312 & 0 & 0 & 0 & 44L & 0 & 108 & 0 & 0 & 0 & -26L & 0 \\ 0 & 312 & 0 & -44L & 0 & 0 & 0 & 108 & 0 & 26L & 0 & 0 \\ 0 & 0 & 280 & 0 & 0 & 0 & 0 & 0 & 140 & 0 & 0 & 0 \\ 0 & -44L & 0 & 8L^2 & 0 & 0 & 0 & -26L & 0 & -6L^2 & 0 & 0 \\ 44L & 0 & 0 & 0 & 8L^2 & 0 & 26L & 0 & 0 & 0 & -6L^2 & 0 \\ 0 & 0 & 0 & 0 & 0 & 0 & 0 & 0 & 0 & 0 & 0 & 0 \\ 108 & 0 & 0 & 0 & 26L & 0 & 312 & 0 & 0 & 0 & -44L & 0 \\ 0 & 108 & 0 & -26L & 0 & 0 & 0 & 312 & 0 & 44L & 0 & 0 \\ 0 & 0 & 140 & 0 & 0 & 0 & 0 & 0 & 280 & 0 & 0 & 0 \\ 0 & 26L & 0 & -6L^2 & 0 & 0 & 0 & 44L & 0 & 8L^2 & 0 & 0 \\ -26L & 0 & 0 & 0 & -6L^2 & 0 & -44L & 0 & 0 & 0 & 8L^2 & 0 \\ 0 & 0 & 0 & 0 & 0 & 0 & 0 & 0 & 0 & 0 & 0 & 0 \end{pmatrix} \quad (41)$$

$$\frac{\mathbf{M}_{T2}^e}{m^T} = \begin{pmatrix} 588 & 0 & 0 & 0 & 77L & 0 & 252 & 0 & 0 & 0 & -63L & 0 \\ 0 & 588 & 0 & -77L & 0 & 0 & 0 & 252 & 0 & 63L & 0 & 0 \\ 0 & 0 & 560 & 0 & 0 & 0 & 0 & 0 & 280 & 0 & 0 & 0 \\ 0 & -77L & 0 & 14L^2 & 0 & 0 & 0 & -63L & 0 & -14L^2 & 0 & 0 \\ 77L & 0 & 0 & 0 & 14L^2 & 0 & 63L & 0 & 0 & 0 & -14L^2 & 0 \\ 0 & 0 & 0 & 0 & 0 & 0 & 0 & 0 & 0 & 0 & 0 & 0 \\ 252 & 0 & 0 & 0 & 63L & 0 & 588 & 0 & 0 & 0 & -77L & 0 \\ 0 & 252 & 0 & -63L & 0 & 0 & 0 & 588 & 0 & 77L & 0 & 0 \\ 0 & 0 & 280 & 0 & 0 & 0 & 0 & 0 & 560 & 0 & 0 & 0 \\ 0 & 63L & 0 & -14L^2 & 0 & 0 & 0 & 77L & 0 & 14L^2 & 0 & 0 \\ -63L & 0 & 0 & 0 & -14L^2 & 0 & -77L & 0 & 0 & 0 & 14L^2 & 0 \\ 0 & 0 & 0 & 0 & 0 & 0 & 0 & 0 & 0 & 0 & 0 & 0 \end{pmatrix} \quad (42)$$

$$\mathbf{M}_{T3}^e = m^T \begin{pmatrix} 280 & 0 & 0 & 0 & 35L & 0 & 140 & 0 & 0 & 0 & -35L & 0 \\ 0 & 280 & 0 & -35L & 0 & 0 & 0 & 140 & 0 & 35L & 0 & 0 \\ 0 & 0 & 280 & 0 & 0 & 0 & 0 & 0 & 140 & 0 & 0 & 0 \\ 0 & -35L & 0 & 7L^2 & 0 & 0 & 0 & -35L & 0 & -7L^2 & 0 & 0 \\ 35L & 0 & 0 & 0 & 7L^2 & 0 & 35L & 0 & 0 & 0 & -7L^2 & 0 \\ 0 & 0 & 0 & 0 & 0 & 0 & 0 & 0 & 0 & 0 & 0 & 0 \\ 140 & 0 & 0 & 0 & 35L & 0 & 280 & 0 & 0 & 0 & -35L & 0 \\ 0 & 140 & 0 & -35L & 0 & 0 & 0 & 280 & 0 & 35L & 0 & 0 \\ 0 & 0 & 140 & 0 & 0 & 0 & 0 & 0 & 280 & 0 & 0 & 0 \\ 0 & 35L & 0 & -7L^2 & 0 & 0 & 0 & 35L & 0 & 7L^2 & 0 & 0 \\ -35L & 0 & 0 & 0 & -7L^2 & 0 & -35L & 0 & 0 & 0 & 7L^2 & 0 \\ 0 & 0 & 0 & 0 & 0 & 0 & 0 & 0 & 0 & 0 & 0 & 0 \end{pmatrix} \quad (43)$$

and

$$m^T = \frac{\rho AL}{840(1 + \phi)^2} \tag{44}$$

2. Rotational mass matrix \mathbf{M}_R^e

$$\mathbf{M}_R^e = \mathbf{M}_{R1}^e + \phi \mathbf{M}_{R2}^e + \phi^2 \mathbf{M}_{R3}^e \tag{45}$$

Here,

$$\mathbf{M}_{R1}^e = m^R \begin{pmatrix} 36 & 0 & 0 & 0 & 3L & 0 & -36 & 0 & 0 & 0 & 3L & 0 \\ 0 & 36 & 0 & -3L & 0 & 0 & 0 & -36 & 0 & -3L & 0 & 0 \\ 0 & 0 & 0 & 0 & 0 & 0 & 0 & 0 & 0 & 0 & 0 & 0 \\ 0 & -3L & 0 & 4L^2 & 0 & 0 & 0 & 3L & 0 & -L^2 & 0 & 0 \\ 3L & 0 & 0 & 0 & 4L^2 & 0 & -3L & 0 & 0 & 0 & -L^2 & 0 \\ 0 & 0 & 0 & 0 & 0 & 0 & 0 & 0 & 0 & 0 & 0 & 0 \\ -36 & 0 & 0 & 0 & -3L & 0 & 36 & 0 & 0 & 0 & -3L & 0 \\ 0 & -36 & 0 & 3L & 0 & 0 & 0 & 36 & 0 & 3L & 0 & 0 \\ 0 & 0 & 0 & 0 & 0 & 0 & 0 & 0 & 0 & 0 & 0 & 0 \\ 0 & -3L & 0 & -L^2 & 0 & 0 & 0 & 3L & 0 & 4L^2 & 0 & 0 \\ 3L & 0 & 0 & 0 & -L^2 & 0 & -3L & 0 & 0 & 0 & 4L^2 & 0 \\ 0 & 0 & 0 & 0 & 0 & 0 & 0 & 0 & 0 & 0 & 0 & 0 \end{pmatrix} \tag{46}$$

$$\mathbf{M}_{R2}^e = m^R \begin{pmatrix} 0 & 0 & 0 & 0 & -15L & 0 & 0 & 0 & 0 & 0 & -15L & 0 \\ 0 & 0 & 0 & 15L & 0 & 0 & 0 & 0 & 0 & 15L & 0 & 0 \\ 0 & 0 & 0 & 0 & 0 & 0 & 0 & 0 & 0 & 0 & 0 & 0 \\ 0 & 15L & 0 & 5L^2 & 0 & 0 & 0 & -15L & 0 & -5L^2 & 0 & 0 \\ -15L & 0 & 0 & 0 & 5L^2 & 0 & 15L & 0 & 0 & 0 & -5L^2 & 0 \\ 0 & 0 & 0 & 0 & 0 & 0 & 0 & 0 & 0 & 0 & 0 & 0 \\ 0 & 0 & 0 & 0 & 15L & 0 & 0 & 0 & 0 & 0 & 15L & 0 \\ 0 & 0 & 0 & -15L & 0 & 0 & 0 & 0 & 0 & -15L & 0 & 0 \\ 0 & 0 & 0 & 0 & 0 & 0 & 0 & 0 & 0 & 0 & 0 & 0 \\ 0 & 15L & 0 & -5L^2 & 0 & 0 & 0 & -15L & 0 & 5L^2 & 0 & 0 \\ -15L & 0 & 0 & 0 & -5L^2 & 0 & 15L & 0 & 0 & 0 & 5L^2 & 0 \\ 0 & 0 & 0 & 0 & 0 & 0 & 0 & 0 & 0 & 0 & 0 & 0 \end{pmatrix} \tag{47}$$

$$\mathbf{M}_{R3}^e = m^R \begin{pmatrix} 0 & 0 & 0 & 0 & 0 & 0 & 0 & 0 & 0 & 0 & 0 & 0 \\ 0 & 0 & 0 & 0 & 0 & 0 & 0 & 0 & 0 & 0 & 0 & 0 \\ 0 & 0 & 0 & 0 & 0 & 0 & 0 & 0 & 0 & 0 & 0 & 0 \\ 0 & 0 & 0 & 10L^2 & 0 & 0 & 0 & 0 & 0 & 5L^2 & 0 & 0 \\ 0 & 0 & 0 & 0 & 10L^2 & 0 & 0 & 0 & 0 & 0 & 5L^2 & 0 \\ 0 & 0 & 0 & 0 & 0 & 0 & 0 & 0 & 0 & 0 & 0 & 0 \\ 0 & 0 & 0 & 0 & 0 & 0 & 0 & 0 & 0 & 0 & 0 & 0 \\ 0 & 0 & 0 & 0 & 0 & 0 & 0 & 0 & 0 & 0 & 0 & 0 \\ 0 & 0 & 0 & 0 & 0 & 0 & 0 & 0 & 0 & 0 & 0 & 0 \\ 0 & 0 & 0 & 5L^2 & 0 & 0 & 0 & 0 & 0 & 10L^2 & 0 & 0 \\ 0 & 0 & 0 & 0 & 5L^2 & 0 & 0 & 0 & 0 & 0 & 10L^2 & 0 \\ 0 & 0 & 0 & 0 & 0 & 0 & 0 & 0 & 0 & 0 & 0 & 0 \end{pmatrix} \tag{48}$$

where

$$m^R = \frac{\rho I_{ds}}{30L(1 + \phi)^2} \tag{49}$$

3. Torsional mass matrix \mathbf{M}_R^e

$$\mathbf{M}_R^e = \frac{\rho I_{pe} l}{6} \begin{pmatrix} 0 & 0 & 0 & 0 & 0 & 0 & 0 & 0 & 0 & 0 & 0 & 0 \\ 0 & 0 & 0 & 0 & 0 & 0 & 0 & 0 & 0 & 0 & 0 & 0 \\ 0 & 0 & 0 & 0 & 0 & 0 & 0 & 0 & 0 & 0 & 0 & 0 \\ 0 & 0 & 0 & 0 & 0 & 0 & 0 & 0 & 0 & 0 & 0 & 0 \\ 0 & 0 & 0 & 0 & 0 & 0 & 0 & 0 & 0 & 0 & 0 & 0 \\ 0 & 0 & 0 & 0 & 0 & 0 & 0 & 0 & 0 & 0 & 0 & 0 \\ 0 & 0 & 0 & 0 & 2 & 0 & 0 & 0 & 0 & 0 & 1 & 0 \\ 0 & 0 & 0 & 0 & 0 & 0 & 0 & 0 & 0 & 0 & 0 & 0 \\ 0 & 0 & 0 & 0 & 0 & 0 & 0 & 0 & 0 & 0 & 0 & 0 \\ 0 & 0 & 0 & 0 & 0 & 0 & 0 & 0 & 0 & 0 & 0 & 0 \\ 0 & 0 & 0 & 0 & 0 & 0 & 0 & 0 & 0 & 0 & 0 & 0 \\ 0 & 0 & 0 & 0 & 0 & 0 & 0 & 0 & 0 & 0 & 0 & 0 \\ 0 & 0 & 0 & 0 & 0 & 0 & 0 & 0 & 0 & 0 & 0 & 0 \\ 0 & 0 & 0 & 0 & 0 & 0 & 0 & 0 & 0 & 0 & 0 & 0 \\ 0 & 0 & 0 & 0 & 1 & 0 & 0 & 0 & 0 & 0 & 0 & 2 \end{pmatrix} \tag{50}$$

Gyroscopic matrix \mathbf{G}^e

$$\begin{aligned} G &= \frac{1}{2} \int_0^l \rho I_{ps} \dot{\theta}_z (\theta_x \dot{\theta}_y - \theta_y \dot{\theta}_x) ds \\ &+ \frac{1}{2} \int_0^l \rho I_{ps} \Omega_i (\theta_x \dot{\theta}_y - \theta_y \dot{\theta}_x) ds \\ &= \frac{1}{2} \rho I_{ps} \Omega_i \int_0^l (q^T N_{b1}^T N_{b2} \dot{q} - q^T N_{b2}^T N_{b1} \dot{q}) ds \end{aligned} \tag{51}$$

$$\mathbf{G}^e = \mathbf{G}_1^e + \phi \mathbf{G}_2^e + \phi^2 \mathbf{G}_3^e \tag{52}$$

$$\mathbf{G}_1^e = m^R \begin{pmatrix} 0 & 36 & 0 & -3L & 0 & 0 & 0 & -36 & 0 & -3L & 0 & 0 \\ -36 & 0 & 0 & 0 & -3L & 0 & 36 & 0 & 0 & 0 & -3L & 0 \\ 0 & 0 & 0 & 0 & 0 & 0 & 0 & 0 & 0 & 0 & 0 & 0 \\ 3L & 0 & 0 & 0 & 4L^2 & 0 & -3L & 0 & 0 & 0 & -L^2 & 0 \\ 0 & 3L & 0 & -4L^2 & 0 & 0 & 0 & -3L & 0 & L^2 & 0 & 0 \\ 0 & 0 & 0 & 0 & 0 & 0 & 0 & 0 & 0 & 0 & 0 & 0 \\ 0 & -36 & 0 & 3L & 0 & 0 & 0 & 36 & 0 & 3L & 0 & 0 \\ 36 & 0 & 0 & 0 & 3L & 0 & -36 & 0 & 0 & 0 & 3L & 0 \\ 0 & 0 & 0 & 0 & 0 & 0 & 0 & 0 & 0 & 0 & 0 & 0 \\ 3L & 0 & 0 & 0 & -L^2 & 0 & -3L & 0 & 0 & 0 & 4L^2 & 0 \\ 0 & 3L & 0 & L^2 & 0 & 0 & 0 & -3L & 0 & -4L^2 & 0 & 0 \\ 0 & 0 & 0 & 0 & 0 & 0 & 0 & 0 & 0 & 0 & 0 & 0 \end{pmatrix} \tag{53}$$

$$\mathbf{G}_2^e = m^R \begin{pmatrix} 0 & 0 & 0 & 15L & 0 & 0 & 0 & 0 & 0 & 15L & 0 & 0 \\ 0 & 0 & 0 & 0 & 15L & 0 & 0 & 0 & 0 & 0 & 15L & 0 \\ 0 & 0 & 0 & 0 & 0 & 0 & 0 & 0 & 0 & 0 & 0 & 0 \\ -15L & 0 & 0 & 0 & 5L^2 & 0 & 15L & 0 & 0 & 0 & -5L^2 & 0 \\ 0 & -15L & 0 & -5L^2 & 0 & 0 & 0 & 15L & 0 & 5L^2 & 0 & 0 \\ 0 & 0 & 0 & 0 & 0 & 0 & 0 & 0 & 0 & 0 & 0 & 0 \\ 0 & 0 & 0 & -15L & 0 & 0 & 0 & 0 & 0 & -15L & 0 & 0 \\ 0 & 0 & 0 & 0 & -15L & 0 & 0 & 0 & 0 & 0 & -15L & 0 \\ 0 & 0 & 0 & 0 & 0 & 0 & 0 & 0 & 0 & 0 & 0 & 0 \\ -15L & 0 & 0 & 0 & -5L^2 & 0 & 15L & 0 & 0 & 0 & 5L^2 & 0 \\ 0 & -15L & 0 & 5L^2 & 0 & 0 & 0 & 15L & 0 & -5L^2 & 0 & 0 \\ 0 & 0 & 0 & 0 & 0 & 0 & 0 & 0 & 0 & 0 & 0 & 0 \end{pmatrix} \tag{54}$$

$$\mathbf{G}_3^e = m^R \begin{pmatrix} 0 & 0 & 0 & 0 & 0 & 0 & 0 & 0 & 0 & 0 & 0 & 0 \\ 0 & 0 & 0 & 0 & 0 & 0 & 0 & 0 & 0 & 0 & 0 & 0 \\ 0 & 0 & 0 & 0 & 0 & 0 & 0 & 0 & 0 & 0 & 0 & 0 \\ 0 & 0 & 0 & 0 & 10L^2 & 0 & 0 & 0 & 0 & 0 & 5L^2 & 0 \\ 0 & 0 & 0 & -10L^2 & 0 & 0 & 0 & 0 & 0 & -5L^2 & 0 & 0 \\ 0 & 0 & 0 & 0 & 0 & 0 & 0 & 0 & 0 & 0 & 0 & 0 \\ 0 & 0 & 0 & 0 & 0 & 0 & 0 & 0 & 0 & 0 & 0 & 0 \\ 0 & 0 & 0 & 0 & 0 & 0 & 0 & 0 & 0 & 0 & 0 & 0 \\ 0 & 0 & 0 & 0 & 0 & 0 & 0 & 0 & 0 & 0 & 0 & 0 \\ 0 & 0 & 0 & 0 & 5L^2 & 0 & 0 & 0 & 0 & 0 & 10L^2 & 0 \\ 0 & 0 & 0 & -5L^2 & 0 & 0 & 0 & 0 & 0 & -10L^2 & 0 & 0 \\ 0 & 0 & 0 & 0 & 0 & 0 & 0 & 0 & 0 & 0 & 0 & 0 \end{pmatrix} \tag{55}$$

Stiffness matrix

$$\mathbf{K}^e = \mathbf{K}_0^e + \phi \mathbf{K}_1^e + \mathbf{K}_2^e, \tag{56}$$

The stiffness matrix of the beam element is written as

where

$$\mathbf{K}_0^e = k_s \begin{pmatrix} 12 & 0 & 0 & 0 & 6L & 0 & -12 & 0 & 0 & 0 & 6L & 0 \\ 0 & 12 & 0 & -6L & 0 & 0 & 0 & -12 & 0 & -6L & 0 & 0 \\ 0 & 0 & 0 & 0 & 0 & 0 & 0 & 0 & 0 & 0 & 0 & 0 \\ 0 & -6L & 0 & 4L^2 & 0 & 0 & 0 & 6L & 0 & 2L^2 & 0 & 0 \\ 6L & 0 & 0 & 0 & 4L^2 & 0 & -6L & 0 & 0 & 0 & 2L^2 & 0 \\ 0 & 0 & 0 & 0 & 0 & 0 & 0 & 0 & 0 & 0 & 0 & 0 \\ -12 & 0 & 0 & 0 & -6L & 0 & 12 & 0 & 0 & 0 & -6L & 0 \\ 0 & -12 & 0 & 6L & 0 & 0 & 0 & 12 & 0 & 6L & 0 & 0 \\ 0 & 0 & 0 & 0 & 0 & 0 & 0 & 0 & 0 & 0 & 0 & 0 \\ 0 & -6L & 0 & 2L^2 & 0 & 0 & 0 & 6L & 0 & 4L^2 & 0 & 0 \\ 6L & 0 & 0 & 0 & 2L^2 & 0 & -6L & 0 & 0 & 0 & 4L^2 & 0 \\ 0 & 0 & 0 & 0 & 0 & 0 & 0 & 0 & 0 & 0 & 0 & 0 \end{pmatrix}, \tag{57}$$

$$\mathbf{K}_1^e = k_s \begin{pmatrix} 0 & 0 & 0 & 0 & 0 & 0 & 0 & 0 & 0 & 0 & 0 & 0 \\ 0 & 0 & 0 & 0 & 0 & 0 & 0 & 0 & 0 & 0 & 0 & 0 \\ 0 & 0 & 0 & 0 & 0 & 0 & 0 & 0 & 0 & 0 & 0 & 0 \\ 0 & 0 & 0 & L^2 & 0 & 0 & 0 & 0 & 0 & -L^2 & 0 & 0 \\ 0 & 0 & 0 & 0 & L^2 & 0 & 0 & 0 & 0 & 0 & -L^2 & 0 \\ 0 & 0 & 0 & 0 & 0 & 0 & 0 & 0 & 0 & 0 & 0 & 0 \\ 0 & 0 & 0 & 0 & 0 & 0 & 0 & 0 & 0 & 0 & 0 & 0 \\ 0 & 0 & 0 & 0 & 0 & 0 & 0 & 0 & 0 & 0 & 0 & 0 \\ 0 & 0 & 0 & 0 & 0 & 0 & 0 & 0 & 0 & 0 & 0 & 0 \\ 0 & 0 & 0 & -L^2 & 0 & 0 & 0 & 0 & 0 & L^2 & 0 & 0 \\ 0 & 0 & 0 & 0 & -L^2 & 0 & 0 & 0 & 0 & 0 & L^2 & 0 \\ 0 & 0 & 0 & 0 & 0 & 0 & 0 & 0 & 0 & 0 & 0 & 0 \end{pmatrix}, \tag{58}$$

and

$$k_s = \frac{EI}{L^3(1 + \phi)} \tag{59}$$

$$\mathbf{K}_2^e = \begin{pmatrix} 0 & 0 & 0 & 0 & 0 & 0 & 0 & 0 & 0 & 0 & 0 & 0 \\ 0 & 0 & 0 & 0 & 0 & 0 & 0 & 0 & 0 & 0 & 0 & 0 \\ 0 & 0 & \frac{EA}{L} & 0 & 0 & 0 & 0 & 0 & -\frac{EA}{L} & 0 & 0 & 0 \\ 0 & 0 & 0 & 0 & 0 & 0 & 0 & 0 & 0 & 0 & 0 & 0 \\ 0 & 0 & 0 & 0 & 0 & \frac{GI_{ps}}{L} & 0 & 0 & 0 & 0 & 0 & -\frac{GI_{ps}}{L} \\ 0 & 0 & 0 & 0 & 0 & 0 & 0 & 0 & 0 & 0 & 0 & 0 \\ 0 & 0 & 0 & 0 & 0 & 0 & 0 & 0 & 0 & 0 & 0 & 0 \\ 0 & 0 & -\frac{EA}{L} & 0 & 0 & 0 & 0 & 0 & \frac{EA}{L} & 0 & 0 & 0 \\ 0 & 0 & 0 & 0 & 0 & 0 & 0 & 0 & 0 & 0 & 0 & 0 \\ 0 & 0 & 0 & 0 & 0 & 0 & 0 & 0 & 0 & 0 & 0 & 0 \\ 0 & 0 & 0 & 0 & 0 & -\frac{GI_{ps}}{L} & 0 & 0 & 0 & 0 & 0 & \frac{GI_{ps}}{L} \end{pmatrix}, \tag{60}$$

Appendix 2

Coefficients of mesh stiffness and damping

$$\mathbf{K}_{11}^m = \begin{pmatrix} c_b^2 s^2 & cc_b^2 s & -c_b s s_b & c_b r_p s^2 s_b & cc_b r_p s s_b & c_b^2 r_p s \\ cc_b^2 s & c^2 c_b^2 & -cc_b s_b & cc_b r_p s s_b & c^2 c_b r_p s_b & cc_b^2 r_p \\ -c_b s s_b & -cc_b s_b & s_b^2 & -r_p s s_b^2 & -c r_p s_b^2 & -c_b r_p s_b \\ c_b r_p s^2 s_b & cc_b r_p s s_b & -r_p s s_b^2 & r_p^2 s^2 s_b^2 & c r_p^2 s_b^2 & c_b r_p^2 s s_b \\ cc_b r_p s s_b & c^2 c_b r_p s_b & -c r_p s_b^2 & c r_p^2 s s_b^2 & c^2 r_p^2 s_b^2 & cc_b r_p^2 s_b \\ c_b^2 r_p s & cc_b^2 r_p & -c_b r_p s_b & c_b r_p^2 s_b & cc_b r_p^2 s_b & c_b^2 r_p^2 \end{pmatrix} \tag{61}$$

$$K_{12}^m = \begin{pmatrix} -c_b^2 s^2 & -c c_b^2 s & c_b s s_b & c_b r_g s^2 s_b & c c_b r_g s s_b & c_b^2 r_g s \\ -c c_b^2 s & -c^2 c_b^2 & c c_b s_b & c c_b r_g s s_b & c^2 c_b r_g s_b & c c_b^2 r_g \\ c_b s s_b & c c_b s_b & -s_b^2 & -r_g s s_b^2 & -c r_g s_b^2 & -c_b r_g s_b \\ -c_b r_p s^2 s_b & -c c_b r_p s s_b & r_p s s_b^2 & r_g r_p s^2 s_b^2 & c r_g r_p s s_b^2 & c_b r_g r_p s s_b \\ -c c_b r_p s s_b & -c^2 c_b r_p s_b & c r_p s_b^2 & c r_g r_p s s_b^2 & c^2 r_g r_p s_b^2 & c c_b r_g r_p s_b \\ -c_b^2 r_p s & -c c_b^2 r_p & c_b r_p s_b & c_b r_g r_p s s_b & c c_b r_g r_p s_b & c_b^2 r_g r_p \end{pmatrix} \tag{62}$$

$$K_{21}^m = \begin{pmatrix} -c_b^2 s^2 & -c c_b^2 s & c_b s s_b & -c_b r_p s^2 s_b & -c c_b r_p s s_b & -c_b^2 r_p s \\ -c c_b^2 s & -c^2 c_b^2 & c c_b s_b & -c c_b r_p s s_b & -c^2 c_b r_p s_b & -c c_b^2 r_p \\ c_b s s_b & c c_b s_b & -s_b^2 & r_p s s_b^2 & c r_p s_b^2 & c_b r_p s_b \\ c_b r_g s^2 s_b & c c_b r_g s s_b & -r_g s s_b^2 & r_g r_p s^2 s_b^2 & c r_g r_p s s_b^2 & c_b r_g r_p s s_b \\ c c_b r_g s s_b & c^2 c_b r_g s_b & -c r_g s_b^2 & c r_g r_p s s_b^2 & c^2 r_g r_p s_b^2 & c c_b r_g r_p s_b \\ c_b^2 r_g s & c c_b^2 r_g & -c_b r_g s_b & c_b r_g r_p s s_b & c c_b r_g r_p s_b & c_b^2 r_g r_p \end{pmatrix} \tag{63}$$

$$K_{22}^m = \begin{pmatrix} c_b^2 s^2 & c c_b^2 s & -c_b s s_b & -c_b r_g s^2 s_b & -c c_b r_g s s_b & -c_b^2 r_g s \\ c c_b^2 s & c^2 c_b^2 & -c c_b s_b & -c c_b r_g s s_b & -c^2 c_b r_g s_b & -c c_b^2 r_g \\ -c_b s s_b & -c c_b s_b & s_b^2 & r_g s s_b^2 & c r_g s_b^2 & c_b r_g s_b \\ -c_b r_g s^2 s_b & -c c_b r_g s s_b & r_g s s_b^2 & r_g^2 s^2 s_b^2 & c r_g^2 s s_b^2 & c_b r_g^2 s s_b \\ -c c_b r_g s s_b & -c^2 c_b r_g s_b & c r_g s_b^2 & c r_g^2 s s_b^2 & c^2 r_g^2 s_b^2 & c c_b r_g^2 s_b \\ -c_b^2 r_g s & -c c_b^2 r_g & c_b r_g s_b & c_b r_g^2 s s_b & c c_b r_g^2 s_b & c_b^2 r_g^2 \end{pmatrix} \tag{64}$$

References

1. Kang MR, Kahraman A (2012) Measurement of vibratory motions of gears supported by compliant shafts. *Mech Syst Signal Process* 29:391–403
2. Ericson TM, Parker RG (2013) Planetary gear modal vibration experiments and correlation against lumped-parameter and finite element models. *J Sound Vib* 332:2350–2375
3. Kahraman A, Singh R (1990) Routes to chaos in a geared system with backlash. *J Acoust Soc Am* 88:S195–S195
4. Kahraman A, Singh R (1990) Non-linear dynamics of a spur gear pair. *J Sound Vib* 142:49–75
5. Li S, Wu Q, Zhang Z (2014) Bifurcation and chaos analysis of multistage planetary gear train. *Nonlinear Dynam* 75:217–233
6. Chen S, Tang J, Wu L (2014) Dynamics analysis of a crowned gear transmission system with impact damping: Based on experimental transmission error. *Mech Mach Theory* 74:354–369
7. Hortel M, Škuderová A (2014) Nonlinear time heteronomous damping in nonlinear parametric planetary systems. *Acta Mech* 225:1–15
8. Lu J-W, Chen H, Zeng F-L, Vakakis A, Bergman L (2014) Influence of system parameters on dynamic behavior of gear pair with stochastic backlash. *Meccanica* 49:429–440
9. Sánchez M, Pleguezuelos M, Pedrero J (2014) Tooth-root stress calculation of high transverse contact ratio spur and helical gears. *Meccanica* 49:347–364
10. Chouksey M, Dutt JK, Modak SV (2012) Modal analysis of rotor-shaft system under the influence of rotor-shaft material damping and fluid film forces. *Mech Mach Theory* 48:81–93
11. Lund JW (1978) Critical Speeds, Stability and Response of a Geared Train of Rotors. *J Mech Des* 100:535–538
12. Iida H, Tamura A, Kikuchi K, Agata H (1980) Coupled torsional-flexural vibration of a shaft in a geared system of rotors: 1st report. *Bull JSME* 23:2111–2117
13. Kahraman A (1994) Planetary gear train dynamics. *J Mech Des* 116:713–720
14. Kahraman A, Ozguven HN, Houser DR, Zakrajsek JJ (1992) Dynamic analysis of geared rotors by finite elements. *J Mech Des* 114:507–514
15. Baud S, Velex P (2002) Static and dynamic tooth loading in spur and helical geared systems-experiments and model validation. *J Mech Des* 124:334–346

16. Baguet S, Velex P (2005) Influence of the nonlinear dynamic behavior of journal bearings on gear-bearing assemblies. *Proc ASME Int Des Eng Tech Conf Comput Inf Eng Conf* 5:735–745
17. Baguet S, Jacquenot G (2010) Nonlinear couplings in a gear-shaft-bearing system. *Mech Mach Theory* 45:1777–1796
18. Kang CH, Hsu WC, Lee EK, Shiau TN (2011) Dynamic analysis of gear-rotor system with viscoelastic supports under residual shaft bow effect. *Mech Mach Theory* 46:264–275
19. Ajmi M, Velex P (2001) A model for simulating the quasi-static and dynamic behavior of double helical gears. In: *MPT... Fukuoka: the JSME international conference on motion and power transmissions*, p 132–137
20. Sondkar P, Kahraman A (2013) A dynamic model of a double-helical planetary gear set. *Mech Mach Theory* 70:157–174
21. Liu C, Qin D, Liao Y (2014) Dynamic model of variable speed process for herringbone gears including friction calculated by variable friction coefficient. *J Mech Des* 136:041006
22. Muszynska A (2005) *Rotordynamics*. Taylor & Francis, Boca Raton
23. Ishida Y, Yamamoto T (2012) *Linear and nonlinear rotordynamics*. Wiley-VCH Verlag GmbH & Co. KGaA, Weinheim
24. Shiau TN, Hwang JL (1993) Generalized polynomial expansion method for the dynamic analysis of rotor-bearing systems. *J Eng Gas Turbines Power* 115:209–217
25. Rao JS, Shiau TN, Chang JR (1998) Theoretical analysis of lateral response due to torsional excitation of geared rotors. *Mech Mach Theory* 33:761–783
26. Nelson H (1980) A finite rotating shaft element using Timoshenko beam theory. *J Mech Des* 102:793–803
27. Harnoy A (2002) *Bearing design in machinery: engineering tribology and lubrication*. CRC Press, New York
28. Friswell MI (2010) *Dynamics of rotating machines*. Cambridge University Press, Cambridge
29. Feng S, Geng H, Yu L (2014) Rotordynamics analysis of a quill-shaft coupling-rotor-bearing system. *Proc Inst Mech Eng, Part C: J Mech Eng Sci*. doi:[10.1177/0954406214543673](https://doi.org/10.1177/0954406214543673)
30. Swanson E, Powell CD, Weissman S (2005) A practical review of rotating machinery critical speeds and modes. *Sound Vib* 39:16–17